Eur. Phys. J. D **4**, 169–179 (1998)

THE EUROPEAN PHYSICAL JOURNAL D

On the analysis of exit-channel effects in three-atom unimolecular reactions

L. Bonnet[a] and J.C. Rayez

Laboratoire de Physicochimie Moléculaire[b], Université Bordeaux 1 and CNRS, 33405 Talence Cedex, France

Received: 18 February 1998 / Revised and Accepted: 4 May 1998

Abstract. The key problem of exit-channel effects in unimolecular reactions, which make Transition State Theory (TST) generally unsuitable for the calculation of product state distributions, is analyzed in the triatomic case ABC $\rightarrow$ AB + C for a total angular momentum equal to zero. The vibrational energy of AB is supposed to be quasi conserved on the way from the transition state (TS) to the products. Moreover, classical mechanics is used for the description of rotational and translational motions. In this frame, batches of trajectories are run on model potential energy surfaces from the TS to the products. Their initial conditions on the dividing surface associated with the TS are not distributed at random but instead, they form curves the shapes of which are guided by physical considerations. The reflection of these curves on hypersurfaces orthogonal to the reaction path provides worthwhile information about the nature of exit-channel effects. It is shown that the modulus of the rotational angular momentum of AB is more likely to decrease than to increase, the amplitude of the variation being larger on the average in the first than in the second case. As a consequence, exit-channel effects cause the rotational state distribution to be colder in the products than at the TS, as observed in the reaction $O_2X \rightarrow O_2 + X\,(X = H, D, T)$. In addition to that, a slight improvement of a model recently developed by the authors allows the description of exit-channel effects in a satisfying way which might be included in TST in order to go beyond the Phase Space Theory (PST) of product state distributions.

PACS. 34.10.+x General theories and models of atomic and molecular collisions and interactions (including statistical theories, transition state, stochastic and trajectory models, etc.) – 34.50.-s Scattering of atoms, molecules, and ions – 82.20.-w Chemical kinetics

1 Introduction

Transition State Theory (TST) is one of the leading theories in the field of chemical reactivity [1]. In a quite simple way compared to a dynamical study, TST provides a satisfying answer to the main question asked by kineticists, *i.e.* how do external parameters like temperature or pressure, affect the rate of a chemical reaction. Moreover, the desire to check the validity of the basic assumptions of TST – like the no recrossing of the transition state – by performing dynamical calculations on model potential energy surfaces, led the researchers to obtain a deep insight, at least within the framework of classical mechanics, into the elementary chemical act that represents the crossing of a transition state (TS) [2].

In the field of reaction dynamics, many workers focus on the way in which the energy of a barrier-less unimolecular reaction is finally distributed among the product degrees of freedom [3–5]. In the case when the excess energy (energy available in the products) is sufficiently low, TST makes possible a straightforward prediction and interpretation of how the kinematics controls the energy partitioning (analogous remarks hold for bimolecular processes of the same nature, *i.e.* without barriers and with low excess energies in both the reagents and the products) [6]. This is due to the fact that (i) TST allows a prediction of the vibrational, rotational and translation energy distributions at the TS, provided that the system loses the memory of initial conditions before dissociating and (ii) these energies are conserved from the TS to the products. In such a case of barrier-less process studied at a low excess energy, TST is usually called Phase Space Theory (PST) [7].

On the other hand, when the excess energy is sufficiently large, there are exit-channel effects [8] – essentially couplings between rotation and translation motions of the nascent products from the TS on – which modify the energy partitioning with respect to the predictions of TST (or PST), as has been clearly shown in the beautiful experiments of Moore *et al.* [4] and also Reisler *et al.* [5]. That we are able to precisely measure the alterations of state distributions caused by the transfers [4] and yet, be unable to give a clear interpretation of these alterations, makes the nature of exit-channel effects one of the topical questions of unimolecular reaction dynamics.

[a] e-mail: speedy@lpct.u-bordeaux.fr
[b] URA 5803

Some attempts were made in the past to include an adiabatic channel assumption in the theory, that is to assume that bending vibrations at the TS correlate adiabatically with free-rotations in the products [9,10]. However, as evidenced in recent calculations on the unimolecular process $O_2H \rightarrow O_2 + H$ [11], strong non adiabaticities are very likely to occur once the TS is crossed.

Recently, we proposed a model of integration of the equations of motion along the free-rotation path (FPI model) [12], *i.e.* the path followed by the system if one suppresses artificially the angular dependence of the potential energy (see Sect. 2). In the case where the velocity of recoil between nascent fragments is sufficiently large at the TS, this model leads to a reasonable expression of the final rotational angular momentum in terms of the dynamical conditions at the TS. However, only part of the trajectories may be described by such a model which has to be improved for a complete description of energy transfers.

As a first step in that direction, we focus the present work on the analysis of exit-channel effects in the simple yet interesting case of three-atom unimolecular processes performed in supersonic beam experiments. Some of the conclusions drawn allow an understanding of the weakness of the model previously evoked and suggest methods to refine it.

The article is organized as follows. In Section 2, we define the initial dynamical conditions of the triatomic system and a number of hypotheses which make tractable the analysis of the dynamics in the exit-channel. In particular, classical mechanics is used as it is reasonable for the description of rotation and translation motions at the molecular level [13]. A model reaction is obtained which allows to grasp some of the complexities of the transfers. Moreover, the main limitation of the FPI model is discussed. In Section 3, the description of the dissociation step is still more simplified in order to circumvent some technical difficulties encountered in the phase space analysis of more realistic systems. The resulting dynamical model allows an insight into the nature of exit-channel effects. A slightly modified version of the FPI model is then deduced which leads to results in good agreement with trajectory calculations. Section 4 deals with the realistic processes $O_2X \rightarrow O_2 + X\,(X = H, D, T)$ and Section 5 concludes.

2 Presentation of the problem

2.1 System of interest

The process of interest is of the type $ABC \rightarrow ABC^* \rightarrow AB + C$. In practice, jet-cooled ABC molecules are optically excited to a pure vibrational level at an energy in excess of the dissociation energy, followed by the unimolecular reaction $ABC^* \rightarrow AB + C$ [4,5]. The energy disposal with respect to the bottom of the product channel is noted E_P. In such experiments, the average magnitude of the total angular momentum **J** is most of the time so low that we keep it at zero [14]. The rotational angular momentum **j** of AB and the orbital angular momentum **L** of C with respect to AB have same modular and opposite directions so that the motion of the three atoms is coplanar.

2.2 Hypotheses

(1) As in the method of Wardlaw and Marcus [13], a semiclassical description of the exit-channel dynamics is adopted; the vibration of AB is quantized whereas its rotation and the translation of C with respect to AB are treated within the framework of classical mechanics. The standard Jacobi coordinates R (distance between C and the center of mass G of AB) and ϕ (angle between GC and AB) are used (see Fig. 1 in Ref. [12]). The hybrid phase space/quantum state for ABC is thus completely defined by a set of five numbers (R, P_R, ϕ, j, n), where P_R is the momentum conjugate to R and n is the vibrational quantum number of AB.

(2) In the interval between the optical excitation and the final dissociation, the energy is supposed to randomize completely over all the degrees of freedom of ABC^*. As a consequence, a microcanonical distribution of the states (R, P_R, ϕ, j, n) is assumed at the TS.

(3) A standard assumption of statistical theories is that the vibrational levels of AB evolve adiabatically from the TS onto the products. For the sake of simplicity, we thus neglect the resulting small variation of the vibrational energy E_V. Hence, the system reduces to a rigid rotor AB interacting with an atom C, the disposal of energy being $E_P - E_V$.

(4) In the exit-channel, the interaction potential energy between the rigid rotor AB and C is approximated by:

$$V_I(R, \phi) = V_R(R) + V_\phi(\phi) \exp(-\alpha(R - R_e)) \qquad (2.1)$$

where $V_R(R)$ is the potential energy along the reaction path, associated with the attractive force between AB and C, $V_\phi(\phi)$ is the potential energy associated with the bending force of ABC and the exponential term accounts for the decrease of the bending force from TS to products (see Ref. [12] for some remarks on the validity of Eq. (2.1)). For the quasi-classical trajectory calculations discussed in the next section, $V_R(R)$ and $V_\phi(\phi)$ are approximated by Lennard-Jones and harmonic functions, respectively given by:

$$V_R(R) = 4D\left(\left(\frac{\sigma}{R}\right)^{12} - \left(\frac{\sigma}{R}\right)^{6}\right) \qquad (2.2)$$

and

$$V_\phi(\phi) = \frac{1}{2}C\phi^2. \qquad (2.3)$$

The parameters of the potential energy are chosen to be: $\alpha = 2.6$ Å^{-1}, $R_e = 1.7$ Å, $D = 3$ eV, $\sigma = 1.5$ Å and $C = 9.853$ eV rd^{-1}. The other parameters used are: $m_A = m_B = m_C = 15$ amu (atomic masses), $r_e = 1.2$ Å (equilibrium distance of AB) and $E_P - E_V = 0.2$ eV. All these values have been selected so as to mimic a realistic process. A contour plot representation of the potential energy is given in Figure 1.

2.3 Exit-channel effects

From the qualitative viewpoint, exit-channel effects can be simply understood from the discussion of three trajectories (a), (b) and (c) displayed in Figure 1.

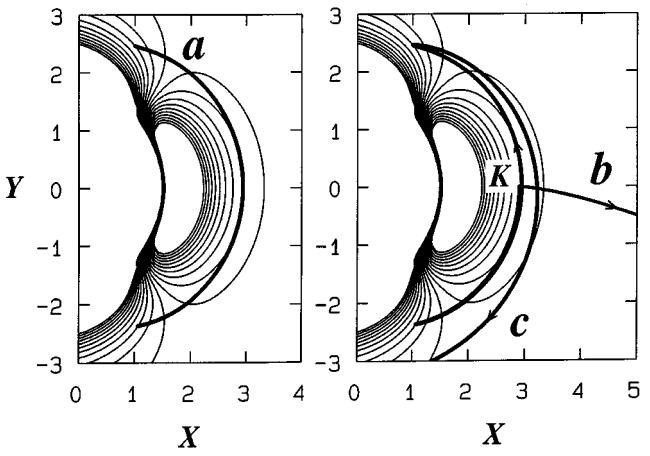

Fig. 1. Contour level representation of the model potential energy given by equations (2.1–2.3). X is equal to $R\cos\phi$ and Y to $R\sin\phi$ (distances are in Å). Contours are equally spaced by 0.1 eV from −1.0 eV to 1.0 eV. Three trajectories (a), (b) and (c) are also represented. Trajectory (a) is the last periodic orbit between the well and the products. The projection of the dividing surface (transition state) on the configuration space coincides with this orbit. Trajectory (b) starts from a point K of the transition state defined by $X = 2.9$ and $Y = 0$, with a large recoil velocity and a small rotational angular momentum. Trajectory (c), which starts from the same point but takes a direction very close to that of the periodic orbit, completes one oscillation before leaving the transition state for good.

Trajectory (a) is a periodic orbit (PO) lying between the well and the products, which corresponds to a bending motion of ABC. We have verified that at the energy considered, there is no other PO between trajectory (a) and the products. In such a case, the TS is then the hypersurface of the phase space (R, P_R, ϕ, j) the projection of which on the configuration space is the same as that of trajectory (a) (see the remarkable chapter written by Pollak in Ref. [2]). In this regard, the TS is often termed *periodic orbit dividing surface* (PODS).

Trajectory (b) leaves the well (from point K in Fig. 1) with a large recoil velocity and corresponds to a weakly-rotating molecule AB from the PODS on. j does not vary significantly en route to products and the transfer of energy from recoil to rotation motion is expected to be small.

Trajectory (c) starts from a state of the PODS which is very close to the external states defining the PO and surrounding any state of the PODS. As a consequence, trajectory (c) follows initially a path in the configuration space which is quite close to that of the PO before taking the direction of the products. Hence, trajectory (c) undergoes one oscillation before dissociating (see Fig. 1). As a matter of fact, the closer to the PO the state from which a trajectory starts, the larger the number of oscillations preceding the final repulsion. In such a case, j varies periodically before taking its asymptotic value – and so does the rotational energy – so that the energy transfer from rotation to translation motion is unpredictable *a priori*.

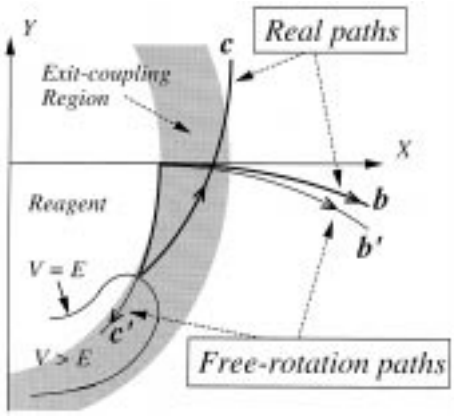

Fig. 2. Scheme displaying two trajectories of type (b) and (c) starting from the TS with a large and low recoil velocity respectively (thick solid lines) as well as the free-rotation paths (b′) and (c′) associated to these trajectories (thin solid lines). The grey area represents the exit-coupling region where most part of the rotational-translational energy transfer takes place.

In a recent note [12], we proposed an analytical formulation of exit-channel effects for trajectories of type (b), which can be summarized as follows. In Figure 2, such a trajectory is represented (path (b)) as well as the trajectory (b') obtained from the same set of dynamical conditions at the TS, with the difference that the bending force constant C is kept at zero in equation (2.3). Trajectory (b') is thus the *free-rotation path* associated to trajectory (b). Our model is based on the simple assumption that integrating the basic equation

$$\frac{dj}{dt} = -\frac{\partial V_I(R,\,\phi)}{\phi} \tag{2.4}$$

along (b') instead of (b) should lead to satisfying results since most part of the transfer responsible for the variation of j takes place in the exit-coupling region where (b) and (b') are very close to each other (grey area in Fig. 2). The main interest of this assumption is that along the free-rotation path, one is able to integrate equation (2.4) analytically (further reasonable hypothesis are needed, however). The resulting expression of the final value j_f of j in terms of the dynamical conditions $(\phi^\ddagger, j^\ddagger)$ at the TS is found to be:

$$j_f = \left(1 - \frac{C^\ddagger}{\alpha^2\nu^2 I^\ddagger}\right) j^\ddagger - \frac{C^\ddagger\phi^\ddagger}{\alpha\nu} \tag{2.5}$$

where the force constant $C^\ddagger$ and the reduced moment of inertia $I^\ddagger$ of the system are given by

$$C^\ddagger = C\exp(-\alpha(R^\ddagger - R_e)) \tag{2.6}$$

and

$$I^\ddagger = \left(\frac{1}{mr_e^2} + \frac{1}{\mu R^{\ddagger 2}}\right)^{-1} \tag{2.7}$$

(m and μ are the reduced masses of AB, and C with respect to AB) and ν is the average recoil velocity in the exit-coupling region (see further below).

The basic limitation of the FPI model is that it cannot be applied just as it is to trajectories of type (c). As a matter of fact, we see in Figure 2 that such trajectories are strongly different from their corresponding free-rotation paths (c') in the exit-coupling region. Due to the very small value of $\dot{R}^{\ddagger}$, the former involve at least one turning point before dissociating whereas the latter reach forbidden areas and are unphysical. This basic limitation of the model appears straightforwardly in equation (2.5). Indeed, ν is very small for trajectories of type (c) so that j_f, which depends on the inverse of ν, may take values not consistent with energy conservation. This is a real problem since the knowledge of the transfer for trajectories of type (c) is necessary for deducing product state distributions from TS ones.

At the present step of the work, it appears necessary to analyze in more details the question of exit-channel effects in order to deduce a model accounting correctly for the trajectories which leave the PODS with a small recoil velocity.

3 An elementary Hamiltonian system

The best way to analyze exit-channel effects is to see how trajectories evolve in the phase space rather than in the configuration space [2]. For this, one solution is to run trajectories from the PODS towards the products and to analyze how the trajectories cross a set of hypersurfaces orthogonal to the reaction path. A consequence of the microcanonical assumption 2 is that the trajectories may start from any point of the PODS with the same density of probability. However, such a distribution of the initial conditions is not a simple task to achieve from the technical viewpoint. This is why we shall consider now an elementary Hamiltonian system which involves the same basic properties as the previous model reaction, but a PODS defined so simply that all the technical problems evoked above are circumvented.

3.1 An elementary Hamiltonian

The Hamiltonian of the system is as follows:

$$H = \frac{\dot{x}^2}{2} + \frac{\dot{y}^2}{2} + e^{-x^2} y^2 = 1. \tag{3.1}$$

The system is thus analogous to the previous one; it involves an oscillator along the coordinate y (corresponding to ϕ) of which the force constant decreases exponentially with the reaction path x (corresponding to R) from $x = 0$ to $x = \infty$. The PODS here is trivially defined by $x = 0$. In the following analysis, $\dot{y}$ is to be compared with j.

3.2 Alteration of a microcanonical distribution in route to products

The microcanonical flux of trajectories through the PODS is given by:

$$F = \int dx dy d\dot{x} d\dot{y}\, \dot{x}\, \delta(x)\, \delta(1 - H)\theta(\dot{x}) \tag{3.2}$$

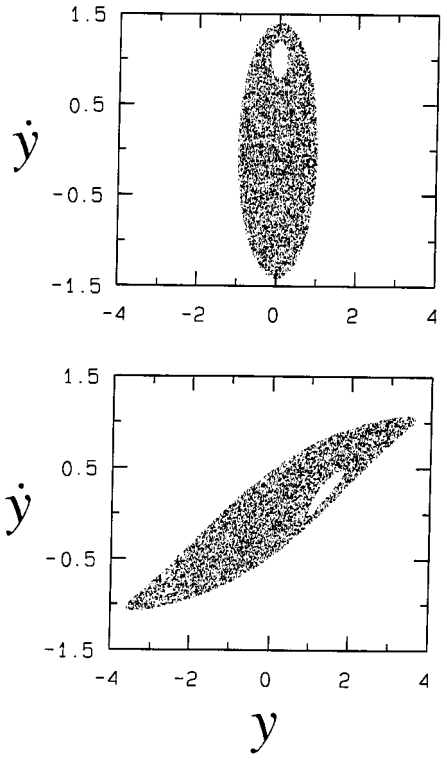

Fig. 3. Upper pannel: microcanonical distribution (5000 points) at the transition state. Lower pannel: reflection of the previous distribution on the hypersurface defined by $x = 4$. Note that the small elliptic area corresponding to a given set of initial conditions at the transition state (upper pannel), is preserved on the way to the products (lower pannel), despite the modification of its contour (Liouville theorem).

which results in

$$F = \int dy d\dot{y}. \tag{3.3}$$

As seen in the above equation, the weight associated with each point $(y, \dot{y})$ of the PODS is equal to 1, due to the canonical nature of the set of coordinates. In other words, the microcanonical distribution is simply a constant in the PODS. Hence, y and $\dot{y}$ are chosen randomly such that the point $(y, \dot{y})$ lies inside the PODS. Then, $\dot{x}$ is deduced from these values, using equation (3.1) (with $x = 0$). Such a distribution is represented in Figure 3 (upper pannel). Its reflection on the hypersurface (HS) defined by $x = 4$ is represented in the same figure (lower pannel). Such representations are comparable with Poincaré sections, with the fundamental difference that one trajectory leads to one point only in both sections [15]. In the lower pannel, (i) the points are still distributed randomly, but (ii) they are no longer surrounded by an ellipse. Point (i) is not surprising. This is just a consequence of the Liouville theorem [16] which states that the flux is conserved along the reaction path. Now, the flux through a given area of the plane $(y, \dot{y})$ is just equal to the area. Hence, a small area of the PODS (upper pannel) leads to the same area

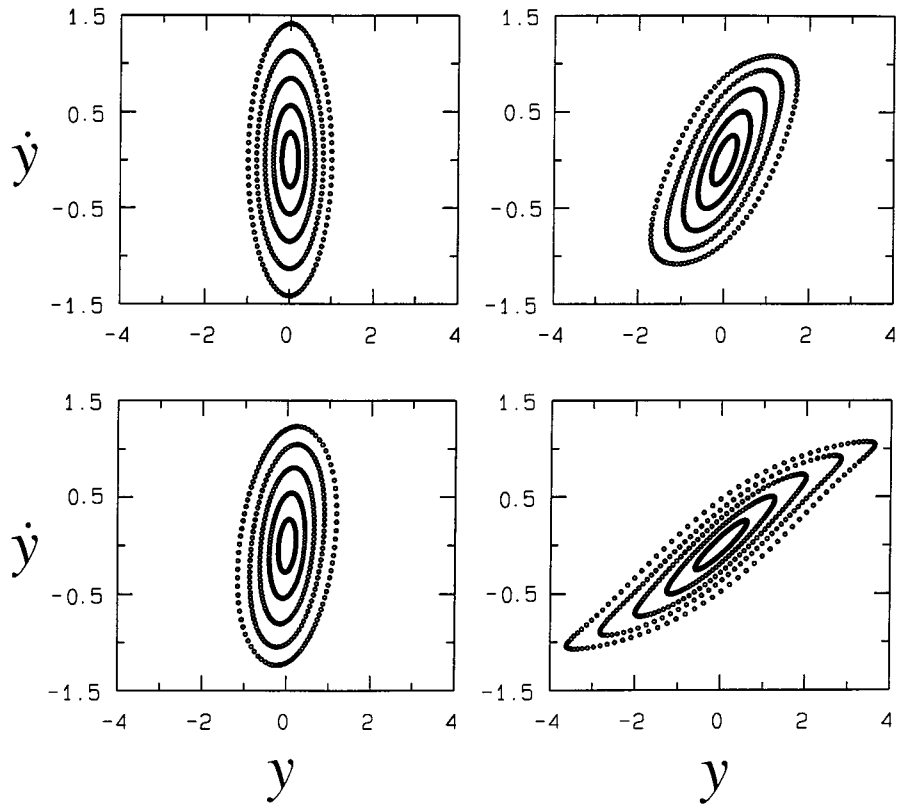

Fig. 4. Representation of five ellipses of the PODS (left top) as well as their reflections on three hypersurfaces respectively defined by $x = 1$ (left bottom), 2.5 (right top) and 4 (right bottom). Each ellipse corresponds to a given value of the velocity $\dot{x}$ at the TS (see text).

in any HS of the exit-channel defined by a given x, with the difference that the shape of the area evolves (lower pannel). The consequence is thus the conservation of a uniform density of points inside the frontier which is an ellipse at the TS and is altered en route to products.

3.3 Implications for TST

Consider for instance $P(\dot{y})$, the product distribution of $\dot{y}$, associated here to j, the modulus of which is measured by the experimentalist. We have

$$P(\dot{y}) = \int \rho(y, \dot{y}) dy \tag{3.4}$$

where $\rho(y, \dot{y})$ is the density of probability that a trajectory crosses a hypersurface HS lying in the products, with y and $\dot{y}$. Since we know from the previous arguments that $\rho(y, \dot{y})$ is uniform inside a closed curve of the HS and is zero outside (see the lower pannel in Fig. 3), we then deduce:

$$P(\dot{y}) = \Delta y(\dot{y}) = y_{max}(\dot{y}) - y_{min}(\dot{y}). \tag{3.5}$$

An important conclusion is that, how the frontier is altered upon passing from the PODS to the products is the only question which one need answer in order to determine the distribution of any variable in the products. A direct consequence is that the number of trajectories necessary to evaluate a product state distribution can be decreased considerably since one needs only consider those starting close to the PO. In the present case, only 100 trajectories are required whereas several thousands are necessary in the standard Monte-Carlo approach.

3.4 Elliptic initial conditions for the analysis of exit-channel effects

The only information provided in Figure 3 is a global transformation of a cloud of points of uniform density upon passing from the PODS to a given HS. Though this information has some value, it is not really satisfying. Rather, one wishes to know the exact correspondence between one point of the PODS, and its reflection on the HS. This can be achieved by choosing the initial conditions of the trajectories such that the resulting points are not distributed at random in the PODS, but form lines. How these lines are transformed will be shown further to provide worthwhile information about exit-channel effects.

The choice of the lines should obviously be guided by physical considerations. For instance, the initial conditions corresponding to a same value of the velocity $\dot{x}$ are defined

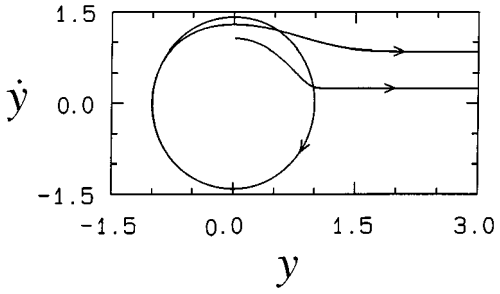

Fig. 5. Paths followed in the plane $(y, \dot{y})$ by two trajectories. The external trajectory which corresponds to $\rho = (1 - 10^{-n})$ with $n = 8$ and $\varphi = \pi/2$ (see Eqs. (3.7, 3.8)), makes two oscillations before leaving the TS for good. The internal trajectory, defined by $\rho = 0.75$ and $\varphi = \pi/2$, leaves the TS directly.

by:

$$y = y_0 = \rho \cos \varphi \tag{3.6}$$

and

$$\dot{y} = \dot{y}_0 = 2^{1/2} \rho \sin \varphi \tag{3.7}$$

where ρ has a given value in the range $[0; 1]$ and φ can take any value in the range $[0; 2\pi]$. The resulting points form an ellipse in the plane $(y, \dot{y})$. The trajectories starting from this ellipse are expected to spend roughly the same period of time in the region where the bending force acts and as a consequence, their motions in the plane $(y, \dot{y})$ should be somewhat similar. In Figure 4 (left top), we have represented five ellipses corresponding to

$$\rho = \frac{i}{5} - 10^{-6} \tag{3.8}$$

i varying from 1 to 5, as well as their reflection on three HS defined by $x = 1$ (left bottom), 2.5 (right top) and 4 (right bottom). As one observes, the five ellipses seem to undergo the same kind of transformation.

Yet, the time spent in the neighborhood of the PO by the trajectories which starts from the external ellipse ($i = 5$), is much larger than the one for the trajectories starting from the internal ellipses ($i = 1{-}4$). Therefore, the previous observation that the transformation is analogous for the five ellipses is somewhat surprising. Indeed, from equations (3.1, 3.6, 3.7), the initial recoil velocity is given by

$$\dot{x}_0 = (2(1 - \rho^2))^{1/2} \tag{3.9}$$

so that, only the values of ρ very close to 1 are consistent with negligible values of $\dot{x}_0$ necessary for the trajectories to remain close to the PO initially. For instance, $\dot{x}_0 = 0.848$ for $i = 4$, which is not negligible with respect to the maximum value 1,414 corresponding to $\rho = 0$. Only for $i = 5$ does $\dot{x}_0$ take the very low value 0.0014.

Actually, the motion of the external trajectories in the plane $(y, \dot{y})$ is quite different from the motion of the internal ones, as shown in Figure 5. The external trajectory which corresponds to $\rho = (1 - 10^{-n})$ with $n = 8$ and $\varphi = \pi/2$ ($y_0 = 0$ and $\dot{y}_0 \sim 2^{1/2}$), makes two oscillations before leaving the TS for good. $\dot{x}$ remains quasi at zero for two periods, and increases suddenly, thus making the repulsion possible. On the other hand, the internal trajectory, defined by $\rho = 0.75$ and $\varphi = \pi/2$ ($y_0 = 0$ and $\dot{y}_0 \sim 1.06$), leaves the TS directly, $\dot{x}_0$ being different from zero.

Despite such a difference of behavior, the final phase of repulsion, occurs roughly in the same way in both cases. Hence, for the external ellipses, there is (i) a first step of rotation motion along the ellipses which remain fixed in the plane $(y, \dot{y})$, and (ii) a second step of "pseudo-rotation" as a whole of the ellipses (see Fig. 4). On the other hand, only the second step does take place for the internal ellipses. Since, however, only the latter step is visible in Figure 4, we understand now why the transformation of the external ellipse seems to be the same as that of the internal ones.

The previous considerations are clearly illustrated in Figure 6 for which the initial conditions form 12 rays distributed regularly. It is seen that their extremities are much more rotated than their origins. To be more precise, the larger ρ, the lower $\dot{x}_0$ (see Eq. (3.9)), the larger the time spent in the neighborhood of the PODS and the larger the rotation. Moreover, we may observe that the alteration of the rays takes place in the very neighborhood of the PODS since in Figure 6b which corresponds to $x = 0.5$, the distortion of the rays is quasi ended. From $x = 0.5$ on (Fig. 6c), there is a pseudo-rotation as a whole as well as a decrease of the major axis of the external ellipse in favour of the minor axis in such a way that the total area is conserved (see also Fig. 4). This transformation is followed by a horizontal translation of the points due to the fact that the velocity $\dot{y}$ is constant. Such a translation is towards the left for the negative values of $\dot{y}$ and towards the right for the positive values.

We note an important fact, *i.e.* the decrease of the maximum of the modulus of $\dot{y}$ from $2^{1/2}$ to ~ 1.1. On the average, the transfer, is thus in favor of $\dot{x}$. Similarly, in a three-atom chemical reaction involving a simple bond fission, the average value of the modulus of j is expected to decrease on the way from the TS onto the products, thus favoring the translational energy as has been observed several times recently [12,17,18].

3.5 On the transformation of the ellipses

To our knowledge, there are no analytical solutions to the equations of motion for the present elementary system. The goal of this section is thus to provide a qualitative explanation of the transformations observed in the previous section. In particular, one wishes to understand the pseudo-rotation as a whole of the internal ellipses observed in Figure 6. This transformation is also the second step of transformation of the external ellipses.

The differential equation relating y to $\ddot{y}$ is

$$\ddot{y} + 2e^{-x^2} y = 0. \tag{3.10}$$

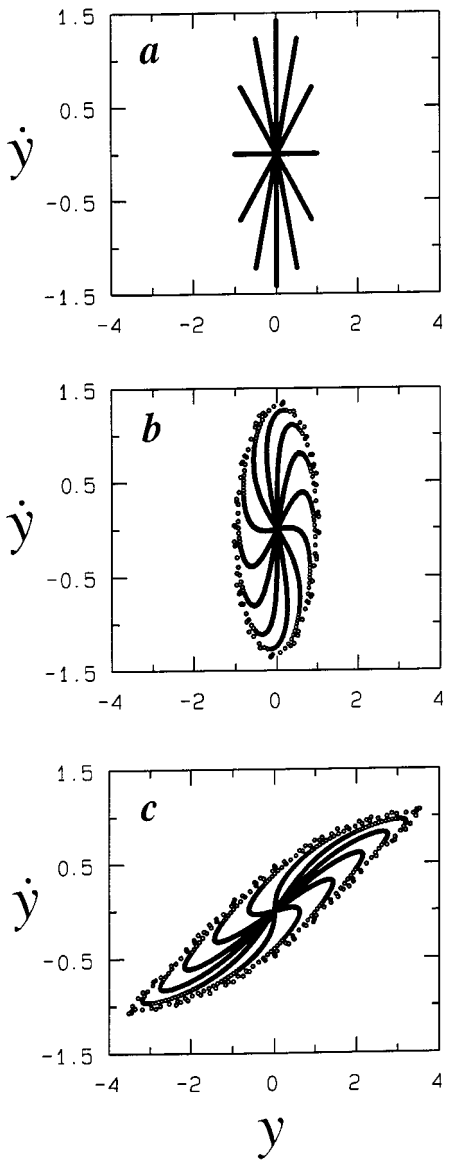

Fig. 6. Representation of twelve rays of the PODS (a) as well as their reflections on two hypersurfaces respectively defined by $x = 0.5$ (b) and 4 (c).

The local frequency $\omega(x)$ of the oscillation for a given x is thus

$$\omega(x) = 2^{1/2} e^{-x^2/2}. \tag{3.11}$$

Let us now consider an internal ellipse E. x and $\omega(x)$ are respectively an increasing and a decreasing function of time. Considering time intervals of small duration δt, one may assume that $\omega(x)$ is a constant over each interval, the value of the constant decreasing suddenly at each change of interval. At time zero, $\omega(x) = \omega_0 = 2^{1/2}$ and in the first interval, $\omega(x) = \omega_1 < \omega_0$ (and so on). Consider at time zero the point of coordinates $(y_0, \dot{y}_0)$. During the first interval, y satisfies to:

$$\ddot{y} + \omega_1^2 y = 0 \tag{3.12}$$

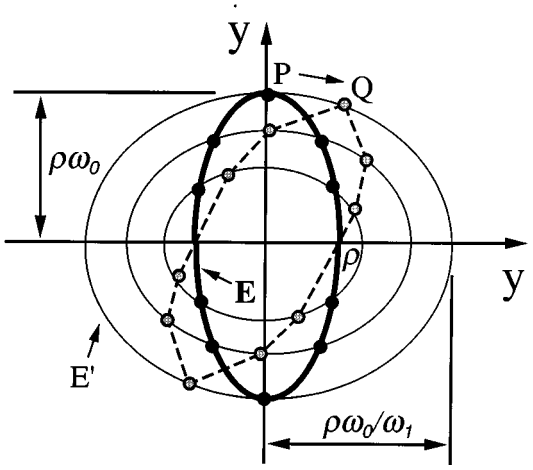

Fig. 7. Schematic representation of the alteration of an internal ellipse over a small period of time (see text).

a general solution of which is

$$y = a\cos(\omega_1 t + \varphi). \tag{3.13}$$

Hence

$$\dot{y} = -a\omega_1 \sin(\omega_1 t + \varphi) \tag{3.14}$$

so that

$$y^2 + \left(\frac{\dot{y}}{\omega_1}\right)^2 = y_0^2 + \left(\frac{\dot{y}_0}{\omega_1}\right)^2. \tag{3.15}$$

Therefore, the path in the plane $(y, \dot{y})$, followed during δt by the trajectory starting from $(y_0, \dot{y}_0)$ at time zero, is an elementary arc of the ellipse defined by:

$$\frac{a_y}{a_{\dot{y}}} = \frac{1}{\omega_1} \tag{3.16}$$

where a_y and $a_{\dot{y}}$ are the axis of the ellipse along y and $\dot{y}$ respectively. Figure 7 depicts the alteration of the ellipse E (bold solid curve). Point P$(0, \rho\omega_0)$ follows the ellipse E′ (external solid curve) defined by $a_y = \rho\omega_0/\omega_1$ and $a_{\dot{y}} = \rho\omega_0$ (one verifies that they satisfy Eq. (3.16)). E′ is broader than E since $\rho\omega_0/\omega_1$ is larger than ρ, which is the value of the y-axis of E. At time δt, the system is at point Q. The same reasoning can be applied to any point of E. The transformation of E leads finally to a quasi-ellipse (dashed curve) (see also Fig. 4). For x larger than ~ 2, $\omega(x)$ is so small that the ratio $a_y/a_{\dot{y}}$ tends to infinity. Thus, all the points follow horizontal paths (see Figs. 4–6).

To conclude the present part, the reason why the modulus $|\dot{y}|$ of $\dot{y}$ decreases on the average is now very clear. As a matter of fact, Figure 7 shows that the top (bottom) of the dashed curve must lie below (above) the top (bottom) of E since no point of the external ellipse E′, which surrounds any grey point, lies above P. This does not mean that exit-channel effects are never in favor of $|\dot{y}|$. Indeed, Figure 8 shows that $|\dot{y}|$ increases in many cases (36% and this result does not depend on ρ). Nevertheless, the maximum increase (0.74) is lower than the maximum decrease

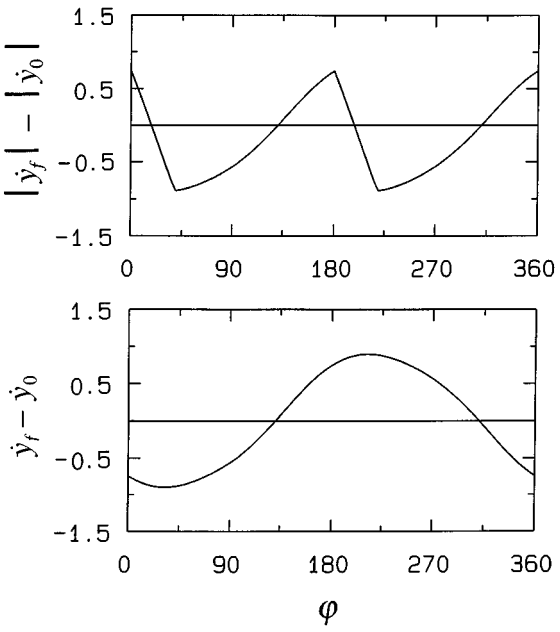

Fig. 8. Value of $(\dot{y}_f - \dot{y}_0)$ (upper pannel) and $(|\dot{y}_f| - |\dot{y}_0|)$ (lower pannel) in terms of φ, the initial phase of the trajectory.

(0.89). On the other hand, $\dot{y}$ has the same probability to increase than to decrease (see Fig. 8). At first sight, such a result may perplex. However, the reader may easily verify that the function $B\cos(\varphi + \varphi_B) - A\cos(\varphi + \varphi_A)$, which may be written as $C\cos(\varphi + \varphi_C)$, has the same probability to be positive than negative over one period whereas the function $|B\cos(\varphi + \varphi_B)| - |A\cos(\varphi + \varphi_A)|$ is more often negative than positive over one period provided that B is lower than A. In the present case, A and B are for a given ellipse, the maximum values of $\dot{y}$ at the TS and in the products respectively so that B is lower than A.

To summarize, exit-channel effects are symmetric with respect to $\dot{y}$, but not with respect to $|\dot{y}|$ which decreases on the average. Since the rotational state distribution is the distribution of the modulus of j (to be compared with $|\dot{y}|$), one may understand why exit-channel effects cause the rotational state distribution to be colder in the products than at the TS.

3.6 Modelling exit-channel effects

As explained in Section 2, the free-path integration model allows the quantification of exit-channel effects for trajectories starting from internal ellipses, *i.e.* far from the PO. Such trajectories leave the PODS with a large velocity of recoil $\dot{x}_0$ (about $2^{1/2}$ in the present case) which makes reasonable the integration of the equations of motion along the free path instead of the real path (see Fig. 2). For the elementary Hamiltonian considered here, the model is as follows; the free path is defined by:

$$x = \dot{x}_0 t \tag{3.17}$$

and

$$y = y_0 + \dot{y}_0 t. \tag{3.18}$$

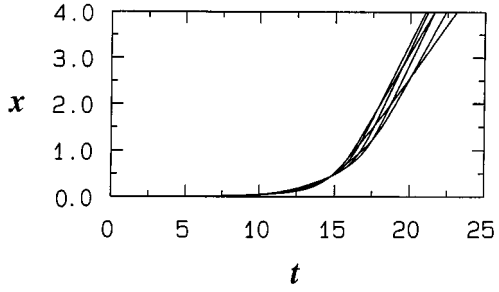

Fig. 9. Time dependence of x for 12 trajectories emerging from points regularly distributed on an external ellipse of the PODS.

Moreover, from equation (3.10), the formal expression of the final value $\dot{y}_f$ of $\dot{y}$ is:

$$\dot{y}_f = \dot{y}_0 - 2\int_0^\infty dt\, e^{-x^2} y. \tag{3.19}$$

From equations (3.17–3.19), we have:

$$\dot{y}_f = \left(1 - \frac{1}{\dot{x}_0^2}\right)\dot{y}_0 - \frac{\pi^{1/2}}{\dot{x}_0} y_0. \tag{3.20}$$

However, we have found that the model leads to results in better agreement with trajectory calculations if one considers the perturbed-path corresponding to the same time dependence of x (see Eq. (3.17)) and:

$$y = y_0 + \dot{y}_0 t + at^2 + bt^3. \tag{3.21}$$

Replacing in equation (3.10), x and y by equations (3.17, 3.21) and owing to the fact that the coefficients of any power of t is equal to zero, one finds:

$$a = -y_0, \quad b = -\frac{\dot{y}_0}{3}\cdot \tag{3.22}$$

Then, equation (3.19) leads to:

$$\dot{y}_f = \left(1 - \frac{1}{\dot{x}_0^2} + \frac{1}{3\dot{x}_0^4}\right)\dot{y}_0 - \left(1 - \frac{1}{2\dot{x}_0^2}\right)\frac{\pi^{1/2}}{\dot{x}_0} y_0. \tag{3.23}$$

In the case of trajectories emerging from external ellipses, $\dot{x}_0$ is very small. From the above equation, it appears clearly that we are dealing with a problem of small divisor which makes FPIM or the related perturbed path integration model (PPIM) unadapted to the description of external trajectories *a priori*.

In Section 3.2, however, it was shown that there is (i) a first step of rotation motion along the external ellipses which remain fixed in the plane $(y, \dot{y})$, and (ii) a second step of "pseudo-rotation" as a whole of these ellipses following a sudden increase of $\dot{x}$ (see Fig. 4). Moreover, this transformation appears to be analogous to that of the internal ellipses. Therefore, during the second step, the time spent in the exit-coupling region by the external trajectories should be approximately the same on the average than the corresponding time for the internal ellipses. In other

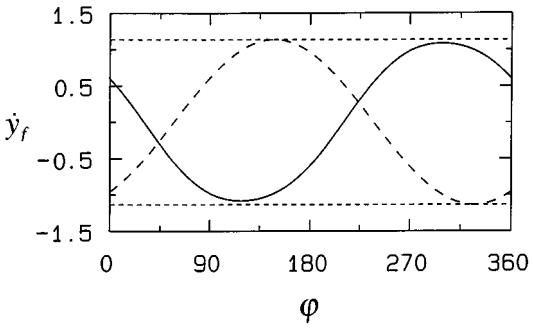

Fig. 10. Value of $\dot{y}_f$ in terms of φ, the initial phase of the trajectory; solid curve: trajectory calculations; dashed curve: PPI model.

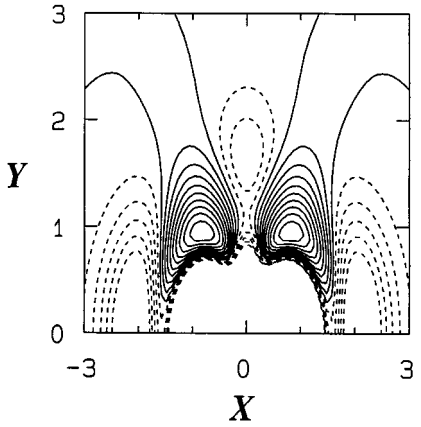

Fig. 11. Contour level representation of the DMBE IV potential energy surface of Pastrana *et al.* for HO_2 (see Ref. [19]), O_2 being kept at its equilibrium distance (1.2 Å). X is equal to $R\cos\phi$ and Y to $R\sin\phi$ (distances are in Å). Contours are equally spaced by 0.2 eV from −1.8 eV to 1.0 eV. Solid curves are for negative values of the potential energy whereas dashed curves are for positive values.

words, the velocity of recoil $\dot{x}$ should be approximately the same on the average for both the external and internal trajectories, *i.e.* about $2^{1/2}$. This is clearly illustrated in Figure 9 where the time dependence of x is given for twelve trajectories starting from points regularly distributed on an external ellipse of the PODS. In the present case, we observe a rather large period of time (13 arbitrary units) corresponding to the first step of rotation motion along the external ellipse, followed by a jump of $\dot{x}$ leading to a quasi linear increase of the x coordinate. The idea is then to "forget" the first step which only modifies the phase φ of the initial conditions given by equations (3.6, 3.7) with $\rho \sim 1$, and to apply equation (3.23) with $\dot{x}_0 = 2^{1/2}$. The maximum $\dot{y}_f$ predicted by the model is 1.25 whereas trajectory calculations lead to 1.08. The transfer is thus underestimated. The reason is that $\dot{x}_0$ cannot be strictly equal to $2^{1/2}$ since all the energy would be in the recoil motion. However, a correction is possible. Since the final value $\dot{x}_f$ of the recoil velocity is related to $\dot{y}_f$ by

$$\dot{x}_f = (2 - \dot{y}_f^2)^{1/2} \tag{3.24}$$

the average value $\bar{\dot{x}}_f$ of $\dot{x}_f$ over the range of initial conditions is given by:

$$\bar{\dot{x}}_f = \frac{1}{2\pi}\int_0^{2\pi} d\varphi\,(2 - \dot{y}_f^2)^{1/2}. \tag{3.25}$$

Replacing $\dot{x}_0$ by $\bar{\dot{x}}_f$ in equation (3.23) and iterating the procedure a small number of times (~ 10), one decreases the maximum value of $\dot{y}_f$ from 1.25 to 1.136, a value in better agreement with 1.08. In Figure 10, the φ-dependence of $\dot{y}_f$ found from trajectories initiated from the external ellipse defined by $\rho = 1 - 10^{-6}$ (solid curve) is compared with the predictions of the PPI model (dashed curve). Due to the phase-shift, only the comparison between the amplitudes of the sinusoidal curves is significant. The close agreement observed tends to show that FPI or PPI models can be applied to describe exit-channel effects at a semi-quantitative level in the case of the simple models considered in the paper.

4 The unimolecular reaction $O_2X \rightarrow O_2 + X$, X = H, D, T

A contour plot representation of the DMBE IV potential energy surface (PES) of Pastrana *et al.* [19] is shown in Figure 11. O_2 is kept at its equilibrium distance (1.2 Å). Solid curves are for negative values of the potential energy and dashed curves are for positive ones. There are two reaction paths connecting two wells with the products. These paths which correspond to values of the Jacobi angle ϕ equal to 55° and 125° respectively, are separated by a hill which is available at the total energy considered. The TS, *i.e.* the dividing surface, has been approximated variationally by using a standard method [13]. The details of the calculations, which are not necessary at the present step of the work, will be given in a subsequent work. The variational dividing surface (VDS) is found to be located at $R^{\ddagger} = 2.115$ Å. Batches of trajectories have been run from this surface. Their initial conditions are as follows; the vibrational energy of O_2 is kept at zero and it has been checked that it does not evolve significantly on the way to the products, thus proving the quasi adiabatic character of the vibration motion. The energy available to the rotation and translation motions is $E_P - E_V = E_P = 0.5$ eV with respect to the products. The initial conditions on the VDS are such that:

$$\frac{j^{\ddagger 2}}{2I^{\ddagger}} + V_I(R^{\ddagger}, \phi^{\ddagger}) = E_P - \frac{1}{2}\mu\nu^{\ddagger 2}. \tag{4.1}$$

Moreover, in the same spirit as previously, we have constrained the recoil velocity to satisfy to the following relation:

$$\frac{1}{2}\mu\nu^{\ddagger 2} = E_P\left(1 - \left(\frac{i}{10}\right)^2\right) \tag{4.2}$$

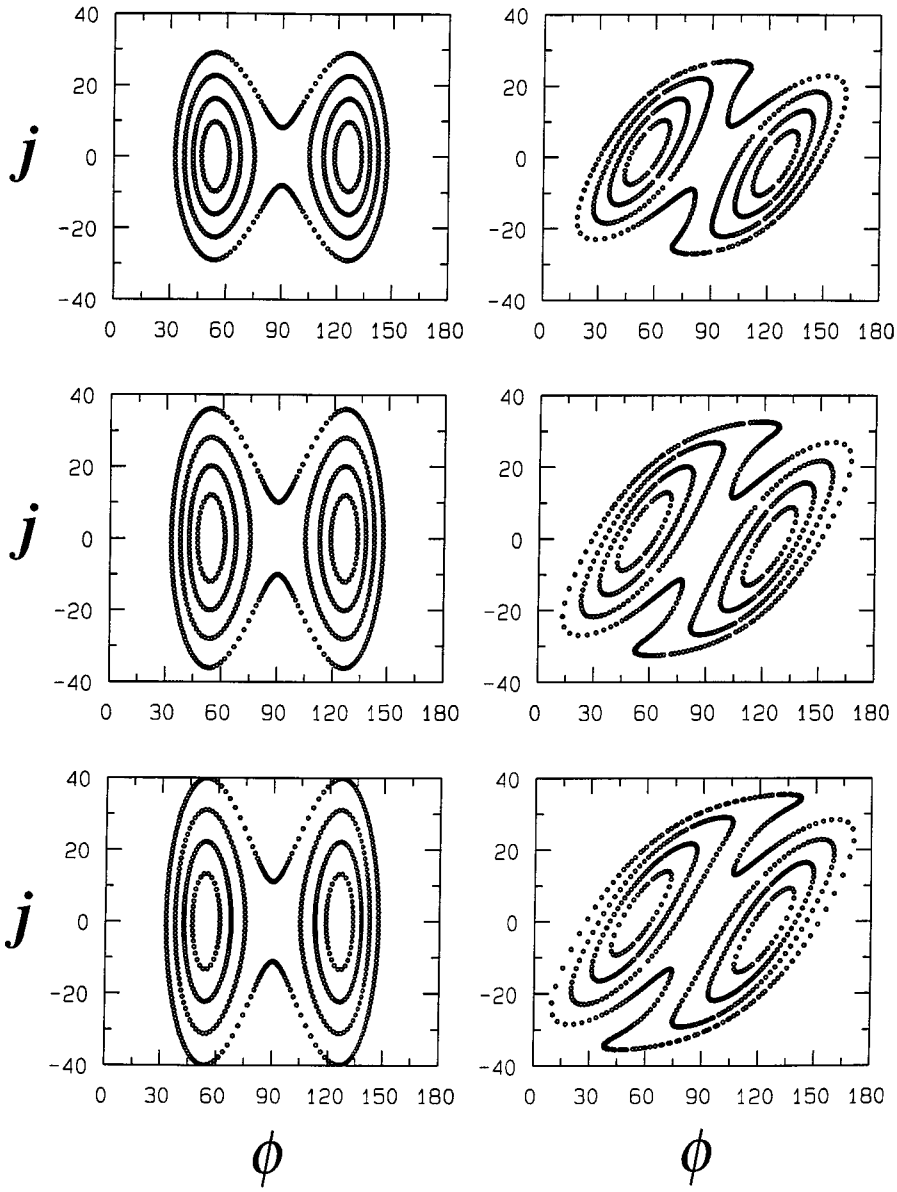

Fig. 12. Representation of four curves of the variational dividing surface defined by $R = 2.115$ Å (left column), as well as their reflections on the hypersurface defined by $R = 4.115$ Å (right column). The three systems considered are O_2H (top), O_2D (middle) and O_2T (bottom).

where i is equal to 3, 5, 7 and 9 respectively. The hypersurface necessary for the analysis of the transfers is placed at $R^{\ddagger} = 4.115$ Å. The results are given in Figure 12 in the three cases X = H, D, T. We have two groups of three quasi-ellipses ($i = 3$, 5, 7) corresponding to velocities of recoil large enough for the trajectories to oscillate around the two reaction paths, thus remaining in the bottom of the exit-channels. In the neighborhood of each reaction path, the bending force may be considered as quasi harmonic so that the behavior observed is just the one analyzed in Section 3 (see Figs. 4 and 6). The shape of the external curve ($i = 9$) is due to the fact that the excess energy is larger than the top of the hill (see Fig. 8). The transformation of this curve is analogous to the one of the internal "ellipses". However, the top and the bottom which correspond to $\phi = 55°$ and 125° are not "rotated" symmetrically. The reason is that the trajectories starting from the top (bottom) do not explore regions of the PES having the same topology than those starting from the bottom (top). The maximum values of the modulus of j for H, D and T are 29, 36 and 40 at the TS (in h unit) and 27, 32.5 and 35.5 in the products. The decrease is thus equal to 2, 3.5 and 4.5 units respectively. As a matter of fact, the larger the mass of the departing atom, the larger the time spent in the interaction region and the larger the rotational-translational energy transfer. In each case, the rotational state distribution appears to be colder in the products than at the TS [18]. However, the shift of the distribution towards the low values of j is small, due to the small masses of H, D and T.

It should be noted that the predictions of the FPI model concerning the maximum final values of j are 27 for H, 33 for D and 36 for T, in close agreement with the QCT results. The weakness of the transfers is certainly responsible for the good agreement found since the lower the transfers, the closer the free-path and the real-path, and the more realistic the model is. The technical details concerning the present application of the FPI model are sufficiently numerous to represent the content of a full paper. They will be given elsewhere.

5 Conclusion

We have analyzed the key problem of exit-channel effects in triatomic unimolecular reactions of the type ABC $\rightarrow$ AB + C for a total angular momentum equal to zero. The vibrational energy of AB has been supposed to be quasi conserved on the way from the transition state TS to the products and classical mechanics has been used for the description of rotational and translational motions. The main findings of the paper are:

(i) in the exit-coupling region, trajectories have a rotation-like motion in the hypersurface (ϕ, j) orthogonal to the reaction path, which is to be related with the nature of the dividing surface, the projection of which on the configuration space coincides with the one of a periodic orbit lying in the exit-channel. In all the cases considered, the excess energy was supposed to be sufficiently large for not having to deal with a multiple TS, *i.e.* with two periodic orbits or more in the exit-channel (the analysis would be much more complicated).

(ii) It is shown that the modulus of the rotational angular momentum of AB is more likely to decrease than to increase, the amplitude of the variation being larger on the average in the first than in the second case. As a consequence, exit-channel effects cause the rotational state distribution to be colder in the products than at the TS. In addition to that, a slight improvement of a model recently developed by the authors (FPIM or PPIM) allows the description of exit-channel effects in a satisfying way and might be included in TST in order to go beyond the Phase Space Theory (PST) of product state distributions.

(iii) The analysis has been done using an elementary Hamiltonian system which allows for circumventing many technical difficulties, but may be considered as being much too simplistic. However, the study of the reaction $O_2X \rightarrow O_2 + X$ (X = H, D, T) with the help of an accurate potential energy surface leads to similar conclusions and supports the idea that the dynamical trends evidenced with our simple Hamiltonian model are of a general nature. In addition to that, the results of the FPI model are in good agreement with the trajectory calculations.

We are very grateful to Dr W. Forst for helpful advices in writing this paper. Learning from the Editors that Roger Grice, deceased on March 11th, 1998, was one of the referees, we decided to dedicate this paper to his memory.

References

1. D.G. Truhlar, B.C. Garrett, S.J. Klippenstein, J. Phys. Chem. **100**, 12771 (1996).
2. E. Pollack, in *Theory of Chemical Reaction Dynamics*, edited by M. Baer (CRC Press, Boca Raton, FL, 1985).
3. See the numerous papers in, Discuss Faraday Soc. **102**, (1995) and Ber. Bunsenges. Phys. Chem. **101**, (1996).
4. E.A. Wade, A. Mellinger, M.A. Hall, C.B. Moore, J. Phys. Chem. A **101**, 6568 (1997); E.A. Wade, H. Clauberg, S.K. Kim, A. Mellinger, C.B. Moore, J. Phys. Chem. A **101**, 732 (1997).
5. I. Nadler, M. Noble, H. Reisler, C. Wittig, J. Chem. Phys. **82**, 2608 (1985); C.X.W. Qian, M. Noble, I. Nadler, H. Reisler, C. Wittig, J. Chem. Phys. **83**, 5573 (1985); C. Wittig, I. Nadler, H. Reisler, J. Catanzarite, G. Radhakrishnan, J. Chem. Phys. **83**, 5581 (1985); S.A. Reid, H. Reisler, J. Phys. Chem. **100**, 474 (1996).
6. L. Bonnet, J.C. Rayez, J. Chem. Phys. **102**, 9512 (1995); J. Phys. Chem. A **101**, 9318 (1997).
7. J.C. Light, J. Chem. Phys. **40**, 3221 (1964); P. Pechukas, J.C. Light, J. Chem. Phys. **42**, 3281 (1965); J.C. Light, J. Lin, J. Chem. Phys. **43**, 3209 (1965); P. Pechukas, J.C. Light, C. Rankin, J. Chem. Phys. **44**, 794 (1966); E.E. Nikitin, *Theory of elementary atomic and molecular proceses in gases*, Sects. 28–31 and 50 (Clarendon Press, Oxford, 1974) and references therein.
8. W.L. Hase, in *Potential Energy Surfaces and Dynamics Calculations*, edited by D. Truhlar (Plenum Press, New York, 1981), pp. 23–24.
9. M. Quack, J. Troe, Ber. Bunsenges. Phys. Chem. **78**, 240 (1974).
10. R.A. Marcus, J. Chem. Phys. **62**, 1372 (1975); G. Worry, R.A. Marcus, J. Chem. Phys. **67**, 1636 (1977).
11. A.J. Dobbyn, M. Stumpf, H.M. Keller, R. Schinke, J. Chem. Phys. **104**, 8357 (1996).
12. L. Bonnet, J.C. Rayez, C. R. Acad. Sci. Paris **IIc**, 101 (1998).
13. D.M. Wardlaw, R.A. Marcus, Adv. Chem. Phys. **70**, 231 (1988).
14. G.A. Brucker, S.I. Ionov, Y. Chen, C. Wittig, Chem. Phys. Lett. **194**, 413 (1992).
15. *Tabor, Chaos and Integrability in Nonlinear Dynamics* (Wiley, New York, 1989).
16. H. Goldstein, *Classical Mechanics*, 2nd edn. (Addison-Wesley Publishing Company, 1980).
17. L. Bonnet, J.C. Rayez, J. Chem. Phys. **103**, 2929 (1995).
18. See Figure 16 in reference [11].
19. M.R. Pastrana, L.A.M. Quintales, J. Brandao, A.J. Varandas, J. Phys. Chem. **94**, 8073 (1990).